Shallow Normal Faulting and Block Rotation Associated with the 1975 Kalapana Earthquake, Kilauea Volcano, Hawaii[1,2]

Eric C. Cannon, Department of Geology, One Shields Avenue, University of California, Davis, CA, 95616; phone: (530) 752-0350
e-mail: cannon@geology.ucdavis.edu

Roland Bürgmann, Department of Geology and Geophysics, 307 McCone Hall, University of California, Berkeley, Berkeley, CA 94720-4767; phone: (510) 643-9545
email: burgmann@seismo.berkeley.edu

Susan E. Owen, Science Hall, Room 125, USC Earth Sciences, Los Angeles, CA 90089-0740; phone: (213) 740-6308
email: owen@earth.usc.edu

(Submitted 05-16-00 to the *Bulletin of the Seismological Society of America*)

[1]More information available at http://perry.geo.berkeley.edu/~burgmann/RESEARCH/research.html
[2]Digital supplemental materials available at ftp://quake.geo.berkeley.edu/outgoing/hawaii/BSSA_2000

Abstract

The Hilina fault system is a set of normal faults located on the south flank of Kilauea Volcano and are thought to accommodate extension within the mobile flank. M>6 earthquakes and aseismic fault slip transport the flank southeastward along a basal detachment at ~8-10 km depth. Only the 1975 M7.2 Kalapana earthquake and the 1868 M7.9 Great Kau have produced slip on the Hilina faults. We analyze Kalapana earthquake fault offsets and observed geodetic displacements to evaluate whether slip on the central Hilina fault system was due to shallow normal faulting independent of basal detachment slip or deep normal faulting dependent on basal detachment slip. Geodetic displacements at the coast are significantly greater than displacements expected from a dislocation model of basal detachment slip. To explain geodetic displacements and fault offsets, we require fault slip on shallow normal faults (as deep as 2-3 km) triggered by slip on the basal detachment. Evidence for block rotation of hanging wall blocks in the central Hilina fault system includes surface displacements values along baselines, subsidence in fault zones determined from line leveling along Chain of Craters Road, and shallow plunges of slip vectors.

Introduction

Several major earthquakes (M≥6) have occurred on the south flank of Kilauea Volcano in historic times (~M7 1823, ~M7.9 1868, M6.5 1954, M7.2 1975, M6.1 1989). These earthquakes are thought to involve slip along an ~8-10-km-deep, subhorizontal basal detachment, driven by rift intrusions and gravitational spreading (Swanson et al., 1976; Dieterich, 1988; Delaney and Denlinger, 1999). The larger events caused extensive surface rupture along the Hilina fault system (Lipman et al., 1985; Wyss, 1988; Bryan, 1992). Hazards associated with major Kilauea earthquakes include significant ground subsidence and tsunamis (Tilling et al., 1975; Lipman et al., 1985, Ma et al., 1999). Major earthquakes could also trigger potentially catastrophic landslides (Moore et al., 1994; Moore and Chadwick, 1995). The M_l=7.2 November 29, 1975 Kalapana earthquake (hereafter referred to as the Kalapana earthquake), the largest south flank earthquake this century, generated a local tsunami 14 m high and produced up to 8 m horizontal displacement seaward and 3.5 m subsidence in coastal regions (Lipman et al., 1985). Similar coastal subsidence was observed following the ~M7.9 1868 Great Kau earthquake (Swanson et al., 1976; Wyss, 1988).

The relationship between slip on the Hilina fault system (Figure 1) and slip on the basal detachment is poorly understood and we study their interaction by comparing observed geodetic displacements, predicted displacements from a dislocation model representing basal detachment slip, and fault offset measurements along the Hilina faults. We find that models of surface displacement due to basal slip alone significantly underestimate observed displacement of coastal geodetic stations along the Hilina fault system. To better explain coastal displacements associated with the Kalapana

earthquake, we present a revised kinematic model requiring slip on shallow Hilina normal faults and the deep basal detachment.

Tectonic Setting

The Kalapana earthquake mainshock and aftershocks, in conjunction with geologic observations, geodetic data, and tsunami studies, provide an improved understanding of faulting behavior of the south flank of Kilauea Volcano. Mainshock focal mechanism studies (Ando, 1979; Furumoto and Kovach, 1979) and observed displacements from geodetic measurements (Lipman et al., 1985; Bürgmann et al., Mechanics of the 1975 Kalapana, Hawaii, earthquake, manuscript in preparation for submission to the *Journal of Geophysical Research*, 2000, hereafter referred to as Bürgmann et al, manuscript in preparation, 2000) indicate southeast transport of the wedge-shaped south flank along an ~8-10-km-deep subhorizontal fault striking approximately northeast. Aftershock activity is primarily confined to a shallowly north-dipping band of microseismicity (Ando, 1979; Got et al., 1994; Gillard et al., 1996). The microseismicity (Figure 2) highlights a weak layer of ocean sediment that separates the mobile south flank block from the Cretaceous Pacific oceanic lithosphere (Hill, 1969; Nakamura, 1980; Thurber and Gripp, 1988). Multiplet relocation of earthquakes collapses a 2-3-km-thick zone into a 100-200-m-thick band of seismicity at 8.5±1.5 km depth, dipping 6°±-4° northward (Got et. al, 1994; Rubin et al., 1999). Bryan (1992) identified a similar concentration of aftershocks at 10 km depth for the 1989 earthquake. Inversions for the 1989 fault rupture plane based on leveling and seismic data coincide with the concentration of aftershocks (Árnadóttir et al., 1991).

Even though the majority of Kalapana earthquake coseismic moment release occurred as subhorizontal slip on the basal detachment, extensive normal faulting was

documented on the surface along the Hilina fault system. Over 25 km of surface rupture occurred along the Hilina fault system from the Kalapana earthquake (Lipman et al., 1985). Lipman et al. (1985) suggested that ~1.5 m of vertical offset along much of the Hilina faults could account for approximately two-thirds of the coastal subsidence, implying that the Hilina fault system played a significant role in south flank deformation associated with the Kalapana earthquake. Kellogg and Chadwick (1987) collected the first detailed fault offset measurements from the Kalapana earthquake and found up to 2.5 m surface offsets (Figure 3). Fault morphology of the Hilina fault system suggests prior fault offset from major earthquakes (Tilling et al., 1976; Cannon and Bürgmann, Prehistoric fault offsets on the Hilina fault system, south flank of Kilauea Volcano, Hawaii, submitted to the *Journal of Geophysical Research*, 2000 hereafter referred to as Cannon and Bürgmann, submitted manuscript, 2000).

The Kalapana earthquake produced a marked change in the style of south flank deformation. From 1896 to the Kalapana earthquake, as much as 1 m northwest-southeast shortening occurred across most of the central south flank region (Swanson et al., 1976). After the Kalapana earthquake, geodetic baselines show contraction across the south flank until about 1981 and extension since then, except during time periods with rift intrusions (Delaney et al., 1998). Between 1983 and 1996, in general the south flank has been rapidly displacing to the southeast with little internal deformation (Delaney et al., 1998; Owen et al., 1995, Owen et al., 1999). Since 1982-1983, the observed displacement field can be modeled as aseismic slip on an 9-km-deep horizontal basal detachment with concurrent rift zone opening between 3 and 9 km depth (Owen et al., 1995). Seismicity rates have not returned to the higher rates observed prior to the Kalapana earthquake (Delaney et al., 1998) suggesting the south

flank is still recovering from the event. Geodetic studies show that the Hilina faults have essentially remained inactive since the Kalapana earthquake (Delaney et al., 1998).

Kinematic Models of the South Flank

The Hilina faults display arcuate, south-facing, normal fault scarps trending east to northeast with a maximum scarp height of ~500 m. Two structural models exist for the Hilina faults, a "shallow" and "deep" model (Figure 2). An ~8-10-km-deep basal detachment and surface expression of the Hilina normal faults are common to both models. However, the "shallow" model treats slip on the Hilina fault system as independent of the basal detachment slip. In the "deep" model, the Hilina faults descend to the basal detachment as normal fault splays. Triggering mechanisms for slip on the Hilina faults may be different for both models. The "shallow" model could produce a greater risk of catastrophic landslides from slip on shallow slump structures than would be associated with the "deep" model of the Hilina fault system.

Several lines of evidence support a shallow fault interpretation. The arcuate surface traces of the Hilina faults resemble spoon-shaped listric normal faults. Riley (1996) conducted a paleomagnetic study of the rotation of lava flows in the Puu Kapukapu block relative to the Hilina Pali fault. In the western Hilina fault system, she proposes that 12°±6° of landward rotation of the Puu Kapukapu block over the last 35.8 ky has occurred on a listric normal fault that extends to a depth of 5.2 km. Ponding of lava flows against the fault scarps also suggests landward rotation of hanging wall blocks (Swanson et al., 1976). A hyaloclastic layer at 1-3 km depth (Swanson et al., 1976) could act as a shallow basal detachment for Hilina faults. Morgan et al. (Confirmation of volcanic spreading models for Kilauea's mobile south flank, Hawaii, from marine

seismic reflection data, in review to Geology, 1999, hereafter referred to as Morgan et al., in review, 1999a; Paua'u seamount: the submarine expression of the active Hilina slump, south flank of Kilauea Volcano, Hawaii, submitted to Journal of Geophysical Research, 1999 hereafter referred to as Morgan et al., submitted manuscript, 1999b) identified seismic reflectors offshore of Halape (Figure 1) at the base of a 2-3-km-thick slump block composed of hyaloclastic material. These reflectors are interpreted as possible subsurface extensions of the Hilina fault system forming a detachment surface beneath the slump block.

The "deep" model presents the Hilina fault system as deeply-rooted normal faults splaying off the ~8-10-km-deep basal detachment (Lipman et al., 1985; Okubo et al., 1997). Microseismicity is detected at 8-10 km depth beneath the upper south flank (Figure 2) possibly representing the splay junction of the deep Hilina Pali fault descending to the basal detachment (Okubo et al., 1996). P-wave tomographic studies show a significant lateral velocity gradient steeply dipping to the southeast beneath the Hilina fault system (Okubo et al, 1996). This velocity gradient, separating low velocity seaward rocks from high velocity inland rocks, may indicate the presence of the Hilina Pali normal fault descending to the basal detachment.

Measurements of Fault Offsets Associated with the Kalapana Earthquake

We analyze ground fractures and geodetic data associated with the Kalapana earthquake to try to understand the mechanisms of displacement for coastal regions. To document the Kalapana earthquake ground fractures, we measure fault offset using piercing point features in fractured 1969-1974 Mauna Ulu lava flows. These flows drape the central Hilina fault system. We measure plunge, azimuth, and magnitude of fault offsets preserved as sawtooth-shaped fractures in Mauna Ulu pahoehoe lava flows.

Fractures are not concentrated along a single fault strand but are distributed over a several 10's-of-meters-wide fracture zone. To measure fault offset across a fracture zone, we sum multiple individual fault offsets along traverses orientated perpendicular to the general trend of the fault scarp. As an example, horizontal offset vector T50 in Figure 3a is calculated by summing 13 individual measurements of horizontal fault offset (labeled "a" through "m"). 73 fault offset traverses contain over 700 individual fault offset measurements (Figure 3; data presented in digital supplemental material Table DSM_1).

We summarize the trend of over 18,000 m of fracture (Digital supplemental material Table DSM_2) and over 200 fault offset measurements (Digital supplemental material Table DSM_ 3) on the Poliokeawe Pali, Holei Pali, and Apua Pali faults in Table 1. Fracture trends and fault offset azimuths are perpendicular to each other within uncertainties for all three faults indicating extension without a lateral shear component. Average fault offset azimuths trend generally southeast, parallel to the south flank displacement associated with the Kalapana earthquake (Figure 1). The largest Kalapana earthquake fault offset for any Hilina fault is located on the Holei Pali where we measured 3.3 m of total offset summed along a traverse of 16 individual measurements.

We assume fractures in the Mauna Ulu lava flows are tectonic in origin resulting from fault slip along the Hilina fault system associated with the Kalapana earthquake. There is no evidence for compressional fold and fault structures at the base of fault scarps, arguing against mass movement as the source of surface fractures. Where safe conditions exist, we descend into fractures to observe the fracture surface. There are no occurrences of slip surfaces parallel or sub-parallel to the bases of lava flows, indicating that the upper few meters of Mauna Ulu pahoehoe lava had not simply detached from

the subsurface to produce surface fractures. Even though fracture azimuth trends (Table 1) are generally parallel to the direction of south flank aseismic displacement and Kalapana earthquake displacement, fractures seem to trend parallel with local fault traces. This parallel relationship and the perpendicular relationship between fracture trace and fault offset suggests that local fault geometry influences the coseismic rupture geometry.

Comparison of Observed and Model Displacements with Fault Offsets

We propose that slip of both the shallow Hilina fault system and the ~8-10-km deep basal detachment slip contribute to coastal displacement associated with the Kalapana earthquake. Our initial kinematic model is schematically illustrated in Figure 4a. The model consists of dislocations that approximate rift zone opening and slip along the basal detachment. No dislocation is included for the Hilina fault system. For a basal detachment slip event, this model predicts that geodetic stations landward or seaward of the Hilina fault system (i.e. on the footwall and hanging wall block of the Hilina fault system) will displace toward the southeast by similar amounts (open vectors in Figure 4a). If in addition to basal detachment slip, secondary slip occurs on the Hilina fault system, geodetic stations on the hanging wall of the Hilina fault system will experience increased observed displacement due to basal detachment slip and slip on the Hilina normal faults. Residuals s1 and s2 (Figure 4a) represent the difference between model and observed geodetic displacement, a value we attribute to slip on the Hilina fault system.

Observed horizontal displacements (solid vectors in Figure 4b, computed from trilateration data) and vertical displacements (solid bars in Figure 4b, from tide gage and leveling data) are calculated relative to geodetic station HVO162 on the footwall of

the central Hilina fault system (Bürgmann et al., manuscript in preparation, 2000). By calculating observed displacements relative to HVO162, motions of coastal geodetic stations on the hanging wall of the Hilina fault system reveal displacement relative to the footwall block. We note that the extension and elevation changes are greatest for coastal geodetic stations situated on the hanging wall blocks of the Hilina fault system. The Hilina footwall block itself moved significantly to the southeast with respect to stations north of Kilauea caldera and the rift zones, as noted by northwest-trending solid vectors of 1-3 m magnitude in Figure 4b.

To separate and evaluate the contributions of the Hilina fault system and basal detachment on the surface displacements, we calculate model displacements as a function of basal detachment slip only (open vectors in Figures 4c and 4d). We utilize model displacements calculated from a variable-slip dislocation model of the Kalapana earthquake derived from an inversion of available geodetic data (reanalysis of trilateration, leveling, and tilt data collected by Hawaiian Volcano Observatory, Lipman et al., 1985). For the inversion, we exclude geodetic data from sites in the hanging wall of the Hilina faults to ensure model displacements are not biased by non-basal detachment slip. Dislocations are included for the basal detachment, east and southwest rift zones, and summit region. The geometry of the basal detachment dislocation was first constrained by inverting for the fault plane geometry using a uniform slip dislocation. The basal detachment dislocation is about 9 km deep at the rift zone, dips 3° to the northwest, and extends 50 km seaward from the rift zone. In the variable-slip inversion, the maximum slip estimated is 17 m and the total moment release is equivalent to a M_w 7.8 earthquake.

Comparison of observed geodetic and model displacements indicates observed displacements significantly exceed model displacements for coastal geodetic stations

(Figures 4c and 4d). Footwall stations (Goat, Goat 2, Pilau-3, Panau) remain stationary relative to HVO162, while Apua Pt2, Kaena Pt, and Laeapuki displace horizontally to the southeast 0.8 to 3.4 m. Horizontal and vertical model displacements for coastal geodetic stations are greatest in the west and decrease for eastern stations. The variable-slip dislocation model predicts uplift at Laeapuki geodetic station. Horizontal geodetic displacements (solid vectors) exceed horizontal model displacement (open vectors) by as much as ~1.5 m. Geodetic measurements of observed subsidence also exceed model displacements by up to ~1.5 m.

In order to compare fault offsets across the central Hilina fault system with observed and model displacements, we identify traverses located near three geodetic baselines. Fault offset traverses (Figure 3) are summed along the GOAT-APUA and H162-KAEN baselines to calculate horizontal and vertical fault offsets across the central Hilina fault system (Figures 4e and 4f). No Mauna Ulu lava flows exist near the PANU-LAEP baseline so no fault offset can be calculated. Solid vectors represent fault offset across the Hilina faults and open vectors are the residual vectors determined by subtracting the model displacements from observed displacements of geodetic data (Figures 4c and 4d). We note that horizontal residual vectors show a transition from southeast to east azimuths for stations farther to the east. The H162-KAEN and PANU-LAEP vertical residual vectors are 18-cm and 16-cm respectively, almost not detectable given the displacement scale in Figure 4f. For both horizontal and vertical fault offset measurements, values exceed corresponding residual vectors by as much as ~1 m. We explain these results in terms of slip on a shallow Hilina fault system and slip along the deep basal detachment for the Kalapana earthquake.

Discussion of Proposed Model

Our efforts provide new data to evaluate the geometry and kinematics of the Hilina fault system. Faulting in the south flank region due to major earthquakes, such as the Kalapana earthquake and probably the Great Kau earthquake, involves slip on Hilina normal faults in addition to slip on the ~8-10-km-deep basal detachment. We support a model of shallow slip for the Hilina fault system in the Kalapana earthquake. First, we comment on our comparison of geodetic displacements, model displacements, and fault offsets. Then we discuss additional support for our shallow fault model interpretation: (1) surface offsets from baseline traverses, (2) line leveling of coseismic elevation changes along the Chain of Craters Road, (3) plunge of slip vectors on Hilina faults; (4) estimates of fault depth for shallow faults. Finally we consider the implications of shallow faulting and propose additional research to evaluate the geometry and kinematics of the Hilina fault system.

Observed displacement of coastal geodetic stations for the Kalapana earthquake cannot be explained by model displacements of basal detachment alone. Horizontal and vertical observed displacements exceed model displacements by as much as ~1.5-m at the surface. This difference indicates secondary slip occurred on the Hilina fault system in the Kalapana earthquake. Probably at least 1.5 m of horizontal slip occurred on the central Hilina fault system at shallow depth since as much as 1.5 m of slip at the surface is suggested. In comparison, maximum predicted displacement on the basal detachment is ~17 m at ~9 km depth. At most, approximately ten times more slip probably occurred on the basal detachment than on the fault surfaces of the Hilina fault system for the Kalapana earthquake.

Traverses across the central Hilina fault system show surface displacements with values up to ~1 m more than residual displacements for both horizontal and vertical components. In other words, surface displacements exceed the minimum estimate of slip contribution from the central Hilina fault system based on residual displacement calculations. Rotation of hanging wall blocks could produce greater surface displacements than geodetic observations for the same baseline across the Hilina fault system. Additional vertical components of surface fault offset produced by hanging wall block rotation cannot be determined from extension of a geodetic baseline if the endpoints of the baseline are distant from the fault scarps. Likewise, collapse of the rollover portion of the hanging wall could produce additional horizontal fault offset not detected in baseline changes. Since the GOAT-APUA and H162-KAEN geodetic baselines both cross at least three traces of fault rupture from the Kalapana earthquake, we conclude block rotation of the hanging wall blocks occurred in the central Hilina fault system.

Line leveling data from the Kalapana earthquake (Lipman et al., 1985) indicates subsidence occurred on the Chain of Craters Road in regions where the road crosses the Holei Pali and Apua Pali faults (Figures 5a and 5.b). Line of section B-B' shows ~1.2 m subsidence in the Holei Pali fault zone and ~0.75 m subsidence in the Apua Pali fault zone relative to HVO162. We interpret this line leveling data to show block rotation of hanging wall blocks of the central Hilina fault system in the Kalapana earthquake (Figure 5c). Since no horizontal position measurement is associated with the leveling data, we cannot calculate the horizontal displacement of these leveling stations due to the Kalapana earthquake; a crucial piece of evidence not available to determine the nature of rotation and deformation of the hanging wall blocks.

To estimate the dip of fault surfaces in the Hilina fault system, we determine the plunge of the slip vector for fault traverses. We utilize the plunge of the slip vector as a proxy for the dip of the fault surface. Values for the plunge of slip vectors for all faults in the central Hilina fault system is 20°±17°. When plunges are grouped by individual fault scarp, values for the plunge of slip vectors on the Poliokeawe Pali, Holei Pali, and Apua Pali faults are 23°±24°, 23°±7°, and 13°±15° respectively (Cannon and Bürgmann, submitted manuscript, 2000). The plunge of the slip vector at the surface probably represents a maximum fault surface dip at depth (Figure 5c). Assuming the Hilina faults shallow at depth, we interpret surface displacements from the GOAT-APUA and H162-KAEN traverses (S_f) to be minimum values of slip at shallow depth (S_s). Displacement observed at HVO162 on the footwall of the Hilina fault system does not represent slip on the shallow Hilina fault system but rather slip on the basal detachment (S_d).

We use plunge estimates from slip vectors to constrain the depth of faulting for the central Hilina fault system (Figure 5c). If the Holei Pali and Apua Pali fault surfaces shallow rapidly with depth, these faults may be less than 1 km deep at the coastline. However, if the fault surfaces maintain a ~20° dip at depth, the fault surface may be 1-2-km deep at the coast. A few km offshore, these fault surfaces may coincide with a seismic reflection layer interpreted as the detachment surface at the base of a 2-3-km-thick slump block composed of hyaloclastic material (Morgan et al., manuscript submitted, 1999b). To the west, the depth of the shallow Hilina fault system may increase as Riley (1996) estimated the depth of the Hilina Pali fault to be 5.2 km.

Our interpretation of the Hilina fault system as a series of shallow normal faults is significant to the development of future kinematic models for mobile volcanic flanks

on Hawaii and elsewhere around the world. The Kalapana earthquake produced slip on two independent fault systems, the basal detachment and the Hilina fault system. Observed displacements of geodetic stations located on the hanging wall of the Hilina fault system should not be used in inversions of basal detachment slip unless dislocations are included to represent the Hilina fault system. Otherwise, the inversion of basal detachment slip will be biased by coastal displacements affected by slip on the Hilina fault system. However, including additional dislocations for the Hilina fault system may not produce a unique model due to limitations imposed by the geodetic network and lack of frequent seismicity in the Hilina fault system. The diminished spatial and temporal resolution of geodetic stations in the past is improving on the south flank with the addition of continuous Global Positioning Station (GPS) sites and application of synthetic-aperture radar image analysis. Precise relocations of microseismicity (Okubo and Got, 1999; Rubin et al., 1999) offer clues to decipher the deeper structure of the south flank. Shallow geophysical exploration techniques, such as land-based seismic reflection and refraction surveys, and borehole logging, would offer the possibility of detecting shallow fault surfaces and landward rotation of subsurface lava flows (Figure 5c) to help constrain kinematic and structural models of the south flank.

Slip on the Hilina fault system plays an undoubtedly important and poorly understood role in the mechanics of the south flank. Understanding the faulting behavior of the south flank directly impacts seismic and tsunami hazard assessment efforts. The reduced fault surface area of a "shallow" rather than "deep" Hilina fault system may require a smaller magnitude seismic event originating deep in the south flank to trigger secondary slip on the Hilina faults. The scenario for triggering a catastrophic submarine landslide originating from the subaerial Hilina fault system is

crucial to assessing the tsunami and landslide potential. Tsunami generation from the Kalapana earthquake probably did not result from slip on the Hilina fault system but rather submarine slumping or basal detachment slip which uplifted the toe region of the south flank block (Ma et al., 1999). However, future earthquakes of M>6 could conceivably produce a catastrophic landslide originating from the Hilina fault system and generate a destructive tsunami.

We hope future work will focus on refining the three-dimensional structure of the Hilina fault system and resolving the effects of Hilina fault slip on geodetic measurements. The implications of a shallow fault geometry for the Hilina fault system must be considered in future earthquake and tsunami hazard assessment for the Hawaiian Islands. Knowledge gained about the stability, structure, and kinematics of the south flank of Kilauea Volcano can be applied to studying and assessing the hazards of other volcanic flanks in the Hawaiian-Emperor volcanic chain and elsewhere around the world.

Conclusions

Detailed mapping and measurement of fault offset in the central Hilina fault system, resulting from the 1975 Kalapana earthquake, helps us understand the role of shallow normal faulting in internal deformation of south flank of Kilauea Volcano, Hawaii. Comparison of observed displacements from geodetic measurements, model displacements of basal detachment slip, and fault offsets supports a kinematic model for the Hilina faults as a set of shallow normal faults. We show that horizontal and vertical observed displacements for coastal geodetic stations are up to ~1.5 m greater than model displacements. Slip on the Hilina fault system, in addition to basal detachment slip, can account for coastal displacements associated with the Kalapana

earthquake. We interpret the central Hilina fault system as a shallow normal fault system, up to 1-2 km deep at the coastline with a maximum depth of 2-3 km, rather than a deep fault system splaying off the basal detachment. We reach this conclusion by evaluating surface fault offsets, plunges of slip vectors, and line leveling data for the Kalapana earthquake. Further work is needed to provide geometric and slip constraints on the Hilina fault system. Accurate structural and kinematic models are fundamental in evaluating seismic and tsunami hazards associated with the Hilina fault system and the mobile south flank block.

Acknowledgements

This work is supported by U. S. Geological Survey National Earthquake Hazards Reduction Program grant 14534-HQ-98-GR-1024 and a Geological Society of America Student Research grant (E.C.C.). Many thanks to folks at Hawaiian Volcano Observatory for assistance, especially Michael Lisowski, Asta Miklius, Arnold Okamura, Don Swanson, and Taeko Jane Takahashi. Peter Cervelli, Sigurjon Jonsson, and Kristine Larson provided assistance during fieldwork. James Kellogg and William Chadwick provided fault offset data from their Hilina fieldwork. Roger Denlinger and Luca Ferrari reviewed an earlier version of this manuscript. We thank our field assistants Jason Bariel, Chad Fleschner, Gwen Pikkarainen, and Jim Weigel for their excellent efforts. The Generic Mapping Tools (GMT) have been invaluable (Wessel and Smith, 1995).

References Cited

Árnadóttir, T., P. Segall, and P. Delaney (1991). A fault model for the 1989 Kilauea south flank earthquake from leveling and seismic data, *Geophys. Res. Lett.* **18**, 2217-2220.

Ando, M. (1979). The Hawaii earthquake of November 29, 1975: Low dip angle faulting due to forceful injection of magma, *J. Geophys. Res.* **94**, no. B13, 7616-7626.

Bürgmann R., S. E. Owen, and P. T. Delaney (2000). Mechanics of the 1975 Kalapana, Hawaii, earthquake, *J. Geophys Res.* (manuscript in preparation for submission).

Bryan, C. J. (1992). A possible triggering mechanism for large Hawaiian earthquakes derived from analysis of the 26 June 1989 Kilauea south flank sequence, *Bull. Seism. Soc. Am*. **82**, no. 6, 2368-2390.

Cannon, E. C. and R. Bürgmann (2000). Prehistoric fault offsets of the Hilina fault system, south flank of Kilauea Volcano, Hawaii, *J. Geophys. Res.* (submitted for publication).

Chadwick Jr., W. W., J. R. Smith Jr., J. G. Moore, D. A. Clague, M. O. Garcia, and C. G. Fox (1993). Bathymetry of south flank of Kilauea Volcano, *U.S. Geol. Surv. Misc. Field Studies*, map MF-2231.

Delaney, P. T. and R. P. Denlinger (1999). Stabilization of volcanic flanks by dike intrusion, an example from Kilauea, *Bull. Volcan*. (in press).

Delaney, P. T., R. Denlinger, M. Lisowski, A. Miklius, P. Okubo, A. Okamura, and M. K. Sako (1998). Volcanic spreading at Kilauea, 1976-1996, *J. Geophys. Res.* **103**, no. B8, 18003-18023.

Denlinger, R. P. and P. Okubo (1995). Structure of the mobile south flank of Kilauea Volcano, Hawaii, *J. Geophys. Res.* **100**, no. B12, 24499-24507.

Dieterich, J. H. (1988). Growth and persistence of Hawaiian volcanic rift zones, *J. Geophys. Res*. **93**, 4258-4270.

Furumoto, A. S., and R. L. Kovach (1979). The Kalapana earthquake of November 28, 1975: An intra-plate earthquake and its relation to geothermal processes, *Phys. Ear. Plan. Int*. **18**, 197-208.

Gillard, D., M. Wyss, and P. Okubo (1996). Type of faulting and orientation of stress and strain as a function of space and time in Kilauea's south flank, Hawaii, *J. Geophys. Res.* **101**, no. B7, 16025-16042.

Got, J.-L., F. W. Fréchet, and W. Klein (1994). Deep fault plane geometry inferred from multiplet relative relocation beneath the south flank of Kilauea, *J. Geophys. Res.* **99**, no. B8, 15375-15386.

Hill, D. P. (1969). Crustal structure of the island of Hawaii from seismic-refraction measurements, *Bull. Seism.Soc. Am.* **59**, no. 1, 101-130.

Hill, D. P. and J. J. Zucca (1987). Geophysical constraints on the structure of Kilauea and Mauna Loa volcanoes and some implications for seismomagmatic processes, *U. S. Geol. Surv. Prof. Pap. 1350,* 903-917.

Kellogg, J. N. and W. Chadwick (1987). Neotectonic study of the Hilina fault system, Kilauea, Hawaii (abstract), *Geol. Soc. Am. Abstracts with Programs* **19**, no. 6, 394.

Lipman, P. W., J. P. Lockwood, R .T. Okamura, D. A. Swanson, and K. M. Yamashita (1985). Ground deformation associated with the 1975 magnitude-7.2 earthquake and resulting changes in activity of Kilauea Volcano, Hawaii, *U. S. Geol. Surv. Prof. Pap. 1276*, 45 pp.

Ma, K.-F., H. Kanamori, and K. Satake (1999). Mechanism of the 1975 Kalapana, Hawaii, earthquake inferred from tsunami data, *J. Geophys. Res.* **104**, no. B6, 13153-13167.

Moore, J. G., W. R. Normark, and R. T. Holcomb (1994). Giant Hawaiian underwater landslides, *Science* **264**, 46-47.

Moore, J. G. and W. W. Chadwick (1995). Offshore geology of Mauna Loa and adjacent areas, Hawaii, *AGU Geophys. Monograph* **92**, 21-44.

Morgan, J. K., G. F. Moore, D. J. Hill, and S. Leslie (1999a). Confirmation of volcanic spreading models for Kilauea's mobile south flank, Hawaii, from marine seismic reflection data, *Geology* (in review).

Morgan, J. K., G. F. Moore, and D. A. Clague (1999b). Papu'u seamount: the submarine expression of the active Hilina slump, south flank of Kilauea Volcano, Hawaii, *J. Geophys. Res*. (submitted for publication).

Nakamura, K. (1980). Why do long rift zones develop better in Hawaiian volcanoes? A possible role of thick ocean sediment, *Bul. Volcano. Soc. Japan* **25**, 255-269.

Okubo, P. G., H. M. Benz, and B. A. Chouet (1997). Imaging the crustal magma sources beneath Mauna Loa and Kilauea volcanoes, Hawaii, *Geology* **25**, no. 10, 867-870.

Okubo, P. G. and J.-L. Got (1999). Constraints on fault geometry based on precise relative relocations of Hawaiian seismicity (abstract), *Eos Trans.* AGU, **80**, no. 17, 666.

Owen, S., P. Segall, J. Freymueller, A. Miklius, R. Denlinger, T. Árnadóttir, M. Sako, and R. Bürgmann (1995). Rapid deformation of the south flank of Kilauea Volcano, Hawaii, *Science* **267**, 1328-1332.

Owen, S., P. Segall, M. Lisowski, A. Miklius, R. Denlinger, J. Freymueller, T. Árnadóttir, T., and M. Sako (2000). The rapid deformation of Kilauea Volcano: GPS measurements between 1990 and 1996, *J. Geophys. Res*. (in press).

Riley, C. (1996). A paleomagnetic study of movement in the Hilina fault system, south flank of Kilauea Volcano, Hawaii (M.S. thesis), Houghton, Michigan Technological University, 61 pp.

Rubin, A. M., Gillard, D., and Got, J.-L. (1999). Streaks of microearthquakes along creeping faults, *Nature* **400**, 635-641.

Swanson, D. A., W. A. Duffield, and R. S. Fiske (1974). Displacement of the south flank of Kilauea Volcano: The result of forceful intrusion of magma into the rift zones, *U. S. Geol. Surv. Prof. Pap. 963*, 39 pp.

Thurber, C. H. and A. E. Gripp (1988). Flexure and seismicity beneath the south flank of Kilauea Volcano and tectonic implications, *J. Geophys. Res.* **93**, no. B5, 4271-4278.

Tilling, R. I.., R. Y. Koyanagi, P. W. Lipman, J. P. Lockwood, J. G. Moore, and D. A. Swanson (1976). Earthquake and related catastrophic events Island of Hawaii, November 29, 1975: A preliminary report, *U. S. Geol. Surv. Circular C 0740*, 33 pp.

Wessel, P. and W. H. F. Smith (1995). New version of the Generic Mapping Tools released, *EOS* **76**, 329.

Wyss, M. (1988). A proposed source model for the Great Kau, Hawaii, earthquake of 1868, *Bull. Seismo. Soc. Am.* **78**, no. 4, 1450-1462.

Figures

Figure 1. Location map of south flank of Kilauea Volcano. Faults of Hilina fault system include Hilina Pali, Puu Kapukapu, Poliokeawe Pali, Holei Pali, and Apua Pali. Star indicates 1975 Kalapana earthquake epicenter. Solid vectors represent horizontal displacement (2-sigma error ellipses) for 1975 Kalapana earthquake calculated from model coordinate solution of available 1974-1976 trilateration data corrected for displacements in a large December 1974 Southwest rift zone intrusion (Bürgmann et al., manuscript in preparation, 2000). Scale vector represents 5 m horizontal displacement. Line of section A-A' in Figure 2.

Figure 2. Northwest-southeast cross-section A-A' of south flank of Kilauea Volcano. Cross-section has no vertical exaggeration. Dots show microseismicity from Gillard et al. (1996); ocean plate geometry from Hill and Zucca (1987). Pelagic sediment layer and thrust faults (dotted lines) interpreted from marine seismic profiles (Morgan et al., submitted manuscript, 1999b). Hilina fault system depicted either as deep normal fault (long-dash line – 75° dip from Okubo et al., 1997) or shallow normal faults (short-dash lines).

Figure 3. Map of (a) horizontal and (b) vertical fault offsets for Kalapana earthquake; error bounds represent summed measurement error of individual piercing points; scale vector is 1 m fault offset. For both maps: solid vectors indicate new data (data presented in Table DSM_1); open vectors indicate data from Kellogg and Chadwick (1987); 1969-1974 Mauna Ulu flows shaded gray; older lava flows shown in white. Inset in (a) shows individual horizontal fault offsets "a" to "m" that are summed to produce horizontal fault offset vector T50. South-trending vectors in (b) represent hanging wall down fault offset.

Figure 4. Model displacements, observed geodetic displacements, and observed fault offsets for Kalapana earthquake. For all figures: horizontal data shown with vectors and vertical data with bars, downward-pointing bars indicates hanging wall down motion; solid symbols indicate observed data; open symbols represent model data. (a) Schematic diagram of contributions of shallow normal faulting and basal detachment slip to observed fault offsets. Triangles represent geodetic stations; solid vectors are measured displacement; open vectors indicate predicted displacements from a coseismic dislocation model of detachment slip computed from data excluding coastal sites. Differences between observed geodetic displacement and model displacement (s1 and s2) are partly attributable to shallow normal faulting. Baseline (BL) fault offset vector represents fault offset at surface calculated from traverses across fault scarps. (b) Observed geodetic displacements calculated relative to HVO162 (Tilling et al., 1975; Lipman et al, 1985). Box outline indicates region for Figures 4c-f. Solid bars represent vertical displacements (tide gage, leveling); solid vectors indicate horizontal EDM (Electronic Distance Measurement) data. (c) and (d) Observed geodetic displacements (solid vectors) and model slip on basal detachment (open vectors) for horizontal (c) and vertical (d) motions (2-sigma error bounds). (e) and (f) Integrated horizontal (e) and vertical (f) fault offsets across Hilina fault system for three baselines. Solid gray vectors and bars (labeled "BL") represent summed surface fault offsets along baselines (error bounds from estimated measurement error); open vectors and bars indicate observed geodetic minus model displacements from basal detachment slip in (c) and (d) (2-sigma error ellipses).

Figure 5. (a) Location map of leveling stations along Chain of Craters Road (CoC). (b) Leveling data from 1975 Kalapana earthquake (Lipman et al., 1985) calculated with respect to HVO162 projected onto line of section B-B'. (c) Schematic

diagram showing possible hanging wall geometry of shallow Hilina fault system along line of section B-B'; cross-section has no vertical exaggeration; dashed lines represent fault surfaces. Dotted lines represent possible dip of lava flows from hanging wall rotation based on paleomagnetic estimates near Puu Kapukapu (Riley, 1996). Slip vector abbreviations are: s_f, slip vector at surface calculated from piercing points; s_s, slip vector on shallow detachment; s_d, slip vector on deep detachment

TABLE 1. Kalapana Earthquake Fracture Characteristics for Hilina Faults

Hilina Fault	Average Fracture Trend* (°)	Average Piercing Point Azimuth* (°)	Horizontal Offset		Vertical Offset	
			Average§ (m) ± σ	Maximum# (m) ± σ	Average§ (m) ± σ	Maximum# (m) ± σ
Polickeawe Pali	088±002	180±008	1.27±0.64	1.95±0.05	-0.16±0.21	-0.53±0.03
Holei Pali	074±003	151±005	1.09±0.85	2.80±0.23	-0.50±0.51	-1.71±0.02
Apua Pali	068±002	155±004	0.35±0.23	0.82±0.02	-0.06±0.13	-0.43±0.04

Uncertainties are given as: * 95% confidence
§ Standard deviation of horizontal or vertical displacements (1-σ)
# Instrument measurement uncertainty (1-σ) for traverse with maximum fault offset

Digital Supplemental Material
Average Fracture Trend data presented in Table DSM_2
Average Piercing Point Azimuth presented in Table DSM_3

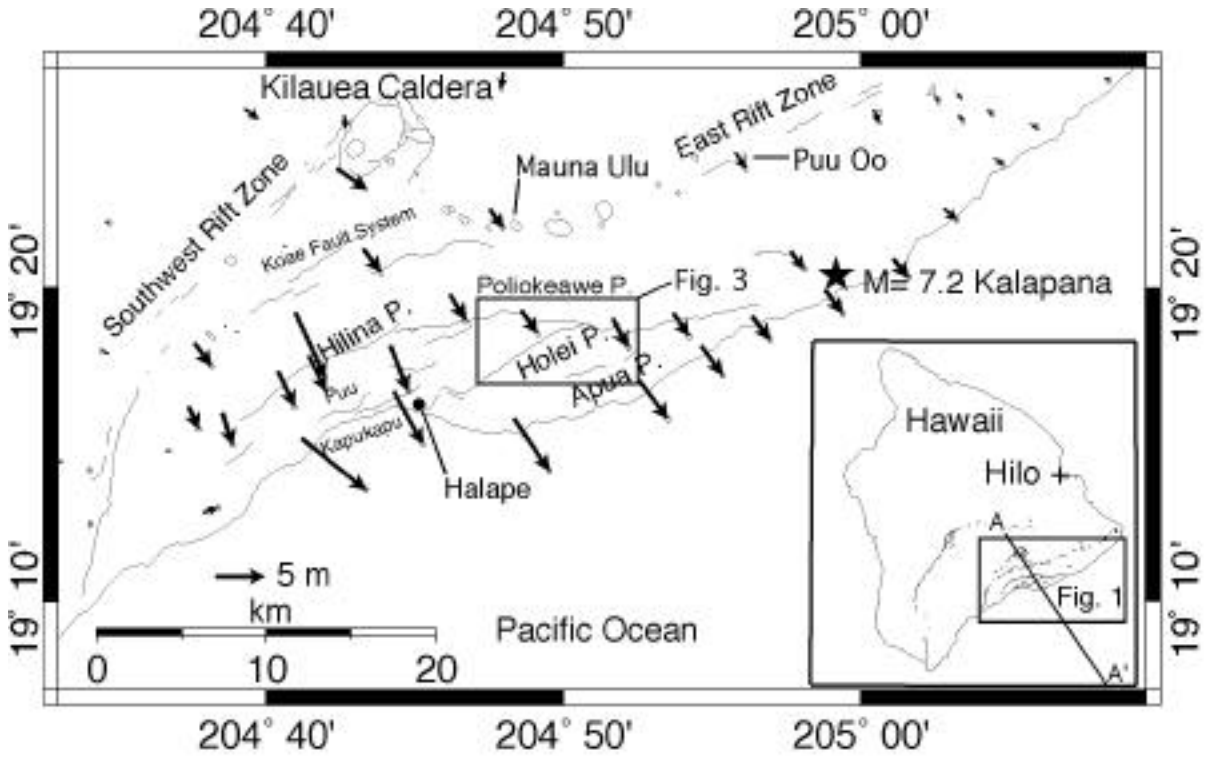
204° 40'
204° 50'
205° 00'
Kilauea Caldera
Mauna Ulu
East Rift Zone
Puu Oo
Southwest Rift Zone
Koae Fault System
Poliokeawe P.
Fig. 3
M= 7.2 Kalapana
Hilina P.
Holei P.
Apua P.
Puu
Kapukapu
Halape
Hawaii
Hilo
A
A'
Fig. 1
5 m
km
0
10
20
Pacific Ocean
19° 20'
19° 10'

Figure 1

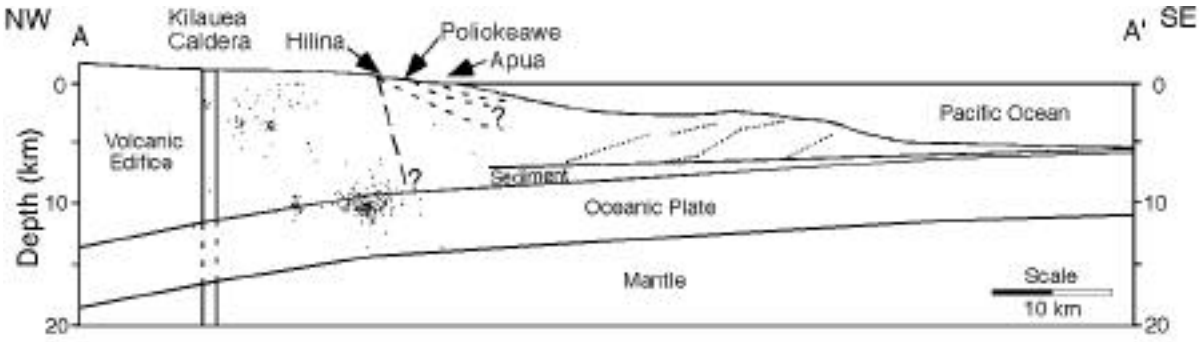
NW
A
Kilauea
Caldera
Hilina
Pelekeawe
Apua
A'
SE
0
10
20
Depth (km)
Volcanic
Edifice
Pacific Ocean
Sediment
Oceanic Plate
Mantle
Scale
10 km

Figure 2

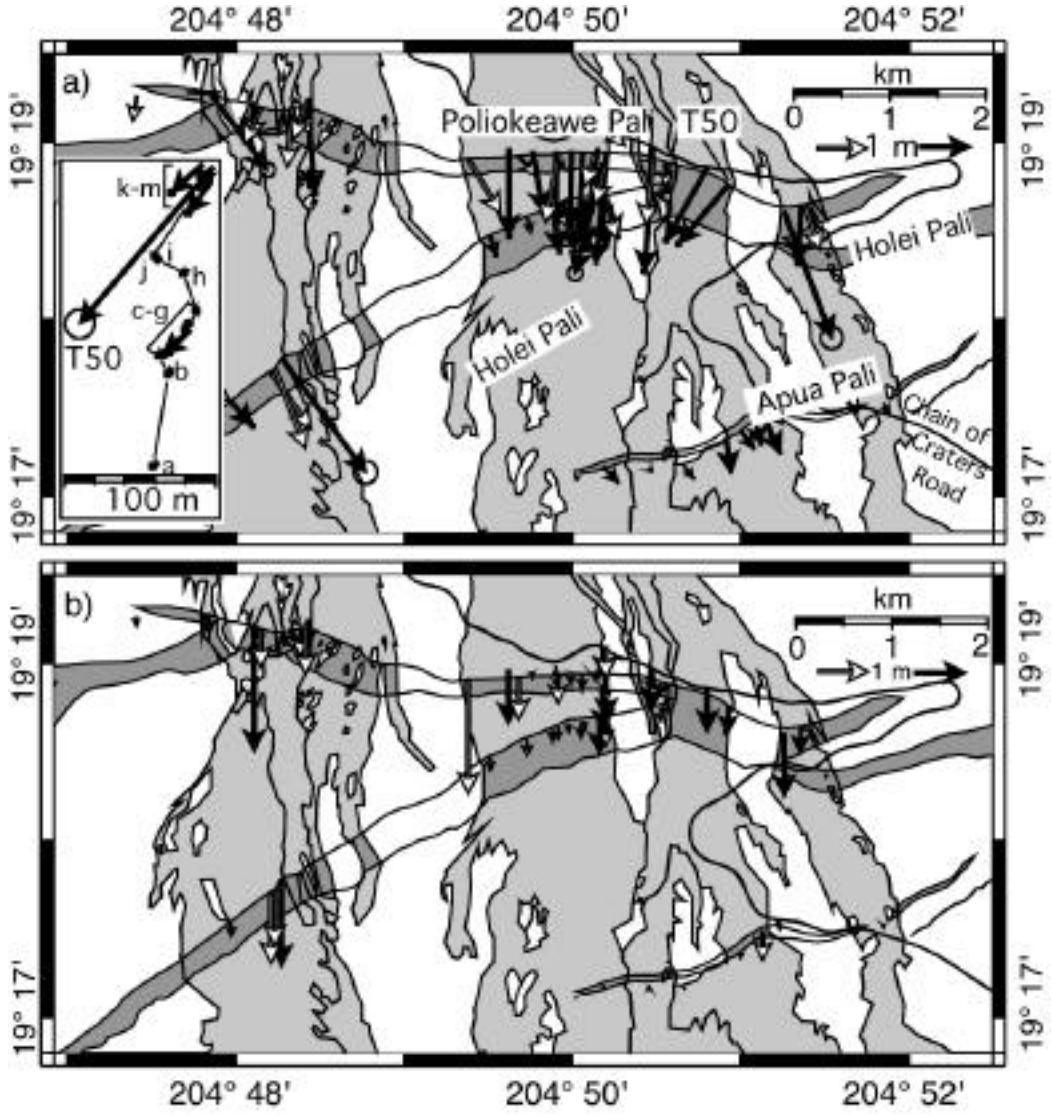
204° 48'
204° 50'
204° 52'
a)
km
0
1
2
1 m
Poliokeawe Pali
T50
Holei Pali
Holei Pali
Apua Pali
Chain of Craters Road
k-m
j
i
h
c-g
T50
b
a
100 m
19° 19'
19° 17'
b)
km
0
1
2
1 m
19° 19'
19° 17'
204° 48'
204° 50'
204° 52'

Figure 3

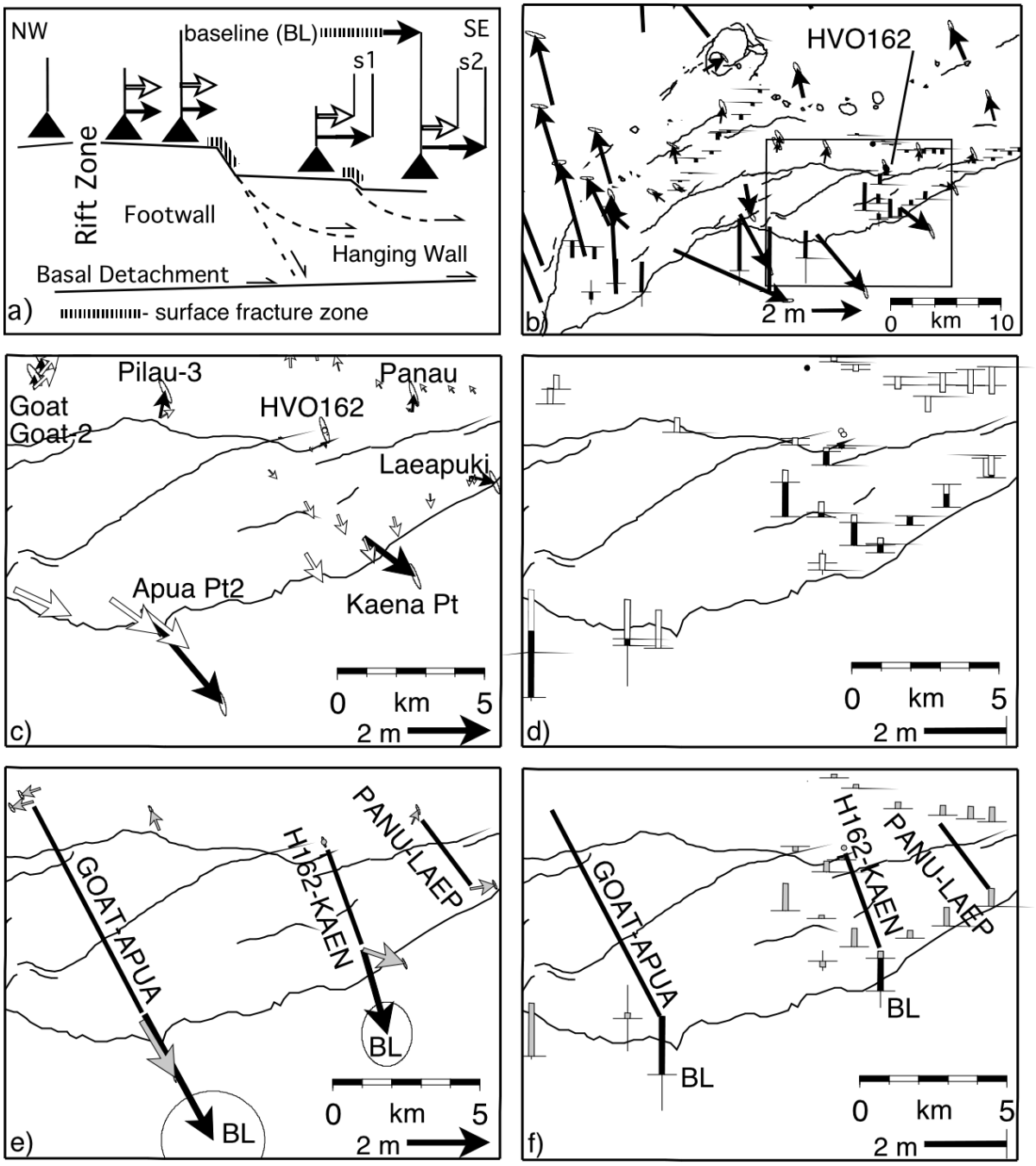
NW
baseline (BL)
SE
s1
s2
Rift Zone
Footwall
Hanging Wall
Basal Detachment
a)
- surface fracture zone
HVO162
2 m
0 km 10
b)
Pilau-3
Panau
Goat
HVO162
Goat-2
Laeapuki
Apua Pt2
Kaena Pt
0 km 5
2 m
c)
0 km 5
2 m
d)
PANU-LAEP
H162-KAEN
GOAT-APUA
BL
0 km 5
2 m
e)
H162-KAEN
PANU-LAEP
GOAT-APUA
BL
BL
0 km 5
2 m
f)

Figure 4

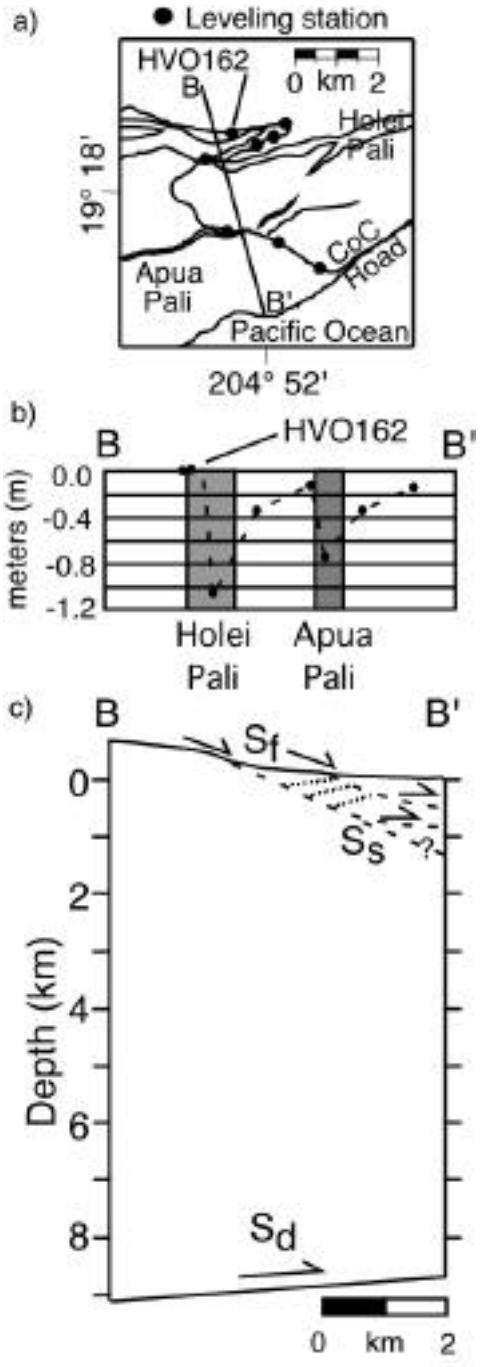
a)
Leveling station
HVO162
B
0 km 2
Holei
Pali
19° 18'
CoC
Road
Apua
Pali
B'
Pacific Ocean
204° 52'
b)
B
HVO162
B'
meters (m)
0.0
-0.4
-0.8
-1.2
Holei
Pali
Apua
Pali
c)
B
B'
Sf
Ss
Depth (km)
0
2
4
6
8
Sd
0 km 2

Figure 5